

Demonstration of soliton self-frequency shift below 1300 nm in higher-order mode, solid silica-based fiber

James van Howe, Jennifer H. Lee, Shian Zhou, Frank Wise, and Chris Xu

School of Applied and Engineering Physics, Cornell University, Ithaca, New York 14853, USA

Siddharth Ramachandran, Samir Ghalmi, and Man F. Yan

OFS Laboratories, 19 Schoolhouse Road, Somerset, New Jersey 08873, USA

Received July 21, 2006; revised October 13, 2006; accepted November 7, 2006;
posted November 9, 2006 (Doc. ID 73273); published January 26, 2007

We demonstrate soliton self-frequency shift of more than 12% of the optical frequency in a higher-order mode solid, silica-based fiber below 1300 nm. This new class of fiber shows great promise for supporting Raman-shifted solitons below 1300 nm in intermediate energy regimes of 1 to 10 nJ that cannot be reached by index-guided photonic crystal fibers or air-core photonic bandgap fibers. By changing the input pulse energy of 200 fs pulses from 1.36 to 1.63 nJ we observe Raman-shifted solitons between 1064 and 1200 nm with up to 57% power conversion efficiency and compressed output pulse widths less than 50 fs. Furthermore, due to the dispersion characteristics of the HOM fiber, we observe redshifted Cerenkov radiation in the normal dispersion regime for appropriately energetic input pulses. © 2007 Optical Society of America
OCIS codes: 190.2640, 190.5530, 190.5940, 060.2280.

The phenomenon of soliton self-frequency shift (SSFS) in optical fiber in which Raman self-pumping continuously transfers energy from higher to lower frequencies¹ has been exploited over the past decade to fabricate widely frequency-tunable, femtosecond pulse sources with fiber delivery.²⁻⁷ Because anomalous (positive) dispersion ($\beta_z < 0$ or $D > 0$) is required for the generation and maintenance of solitons, early sources that made use of SSFS for wavelength tuning were restricted to wavelength regimes greater than 1300 nm where conventional silica fibers exhibited positive dispersion.^{2,3} The recent development of index-guided photonic crystal fibers (PCFs) and air-core photonic bandgap fibers (PBGFs) relaxed this requirement with the ability to design large positive waveguide dispersion and therefore large positive net dispersion in optical fibers at nearly any desired wavelength.⁸ This allowed for a number of demonstrations of tunable SSFS sources supporting input wavelengths as low as 800 nm in the anomalous dispersion regime.⁴⁻⁷

Unfortunately, the pulse energy required to support stable Raman-shifted solitons below 1300 nm in index-guided PCFs and air-core PBGFs is either on the very low side, a fraction of a nanojoule for silica-core PCFs,^{5,6} or on the very high side, greater than 100 nJ (requiring an input from an amplified optical system) for air-core PBGFs.⁷ The low-energy limit is due to high nonlinearity in the PCF. To generate large positive waveguide dispersion to overcome the negative dispersion of the material, the effective area of the fiber core must be reduced. For positive total dispersion at wavelengths less than 1300 nm, this corresponds to an effective area, A_{eff} , of 2–5 μm^2 , approximately an order of magnitude less than conventional single-mode fibers (SMFs). The high-energy limit is due to low nonlinearity in the air-core PBGF where the nonlinear index, n_2 , of air is roughly 1000

times less than that of silica. These extreme ends of nonlinearity dictate the required pulse energy (u) for soliton propagation, which scales as $U \sim D A_{\text{eff}}/n_2$. In fact, most microstructure fibers and tapered fibers with positive dispersion are intentionally designed to demonstrate nonlinear optical effects at the lowest possible pulse energy, while air-core PBGFs are often used for applications that require linear propagation, such as pulse delivery. For these reasons, previous work using SSFS below 1300 nm were performed at soliton energies either too low or too high (by at least an order of magnitude) for many practical applications, such as multiphoton imaging, where bulk solid-state lasers are currently the mainstay for the excitation source.⁹

In this Letter we demonstrate SSFS from 1064 to 1200 nm with up to 57% power efficiency in a higher-order mode (HOM) fiber.¹⁰ This new class of fiber shows great promise for generating Raman solitons in intermediate energy regimes of 1 to 10 nJ pulses that cannot be reached through the use of PCFs and PBGFs. The HOM fiber used in our experiments was recently shown to exhibit large positive dispersion (~ 60 ps/nm km) below 1300 nm while still maintaining a relatively large effective area of 44 μm^2 ,¹⁰ ten times that of index-guided PCFs for similar dispersion characteristics. Through soliton shaping and higher-order soliton compression within the HOM fiber, we are able to generate clean 49 fs pulses from 200 fs input pulses. Due to the dispersion characteristics of the HOM fiber, we also observe redshifted Cerenkov radiation in the normal dispersion regime for appropriately energetic input pulses.

Figure 1(a) shows the dispersion curve for the LP₀₂ mode in the HOM fiber used in our experiment. To generate positive dispersion below 1300 nm while simultaneously maintaining a large effective area, light propagates solely in the LP₀₂ mode. Light is

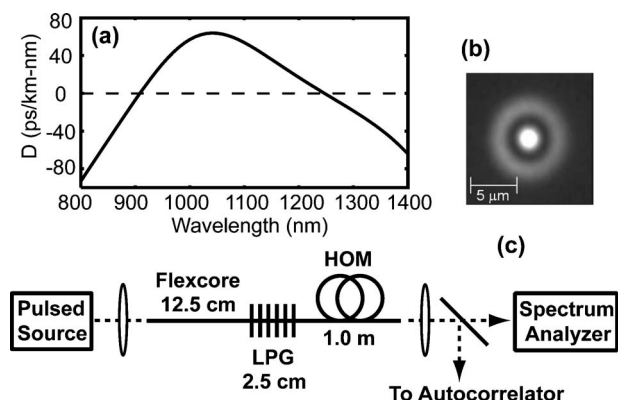


Fig. 1. (a) Total dispersion for propagation in the LP_{02} mode. (b) Experimental near-field image of the LP_{02} mode with effective area $A_{\text{eff}}=44 \mu\text{m}^2$. (c) Experimental setup used to couple light through the HOM fiber module.

coupled into the LP_{02} mode using a low-loss long period grating¹¹ (LPG). The index profile of the HOM fiber is made such that the mode becomes more confined to the higher-index core with an increase in wavelength, resulting in net positive dispersion.¹⁰ Figure 1(a) shows a dispersion of 62.8 ps/nm km at 1060 nm, which is comparable with that of microstructured fibers used previously for SSFS,⁴⁻⁶ and exhibits two zero dispersion wavelengths at 908 and 1247 nm. The mode profile at the end face of the HOM fiber is shown in Fig. 1(b), demonstrating a clean higher-order LP_{02} mode and an effective area of $44 \mu\text{m}^2$. A schematic of the fiber module used for this experiment is shown in Fig. 1(c). Here light propagates in the fundamental mode through 12.5 cm of standard SMF (flexcore) before being coupled into 1.0 m of the HOM fiber with a 2.5 cm LPG (entirely contained within a fiber fusion-splicing sleeve). Light resides in the LP_{01} mode for about half the length of the grating after which more than 99% is coupled into the LP_{02} mode. The module has a total loss of 0.14 dB, which includes all splices, fiber loss, and mode conversion. We also note that the all-silica HOM fiber leverages the standard silica fiber manufacturing platform and retains the low-loss properties (for both transmission and bending) of a conventional SMF, allowing easy termination and splicing.

The experimental setup is shown in Fig. 1(c). The pump source consisted of a fiber laser (Fianium FP1060-1S) that delivered a free space output of ~ 200 fs pulses at a center wavelength of 1064 nm and an 80 MHz repetition rate. We were able to couple a maximum power of 130 mW into the fiber module, corresponding to 1.63 nJ input pulses. Using a variable attenuator, the input pulse energy was varied from 1.36 to 1.63 nJ to obtain clean spectrally shifted solitons with a maximum wavelength shift of 136 nm (12% of the carrier wavelength) as shown in Fig. 2(a). Theoretical traces from numerical simulation for similar input pulse energy are plotted adjacent to the experimental data in Fig. 2(d). We used the split-step Fourier method in our simulation and included self-phase modulation, stimulated Raman scattering, self-steepening, and dispersion up to fifth

order. We obtained the dispersion coefficients by numerically fitting the experimental curve in Fig. 1(a) and used a nonlinear parameter $\gamma=2.2 \text{ W}^{-1} \text{ km}^{-1}$ and a Raman response of $T_R=5 \text{ fs}$.¹² We also approximated the irregularly shaped spectrum of our input source [Fig. 1(b)] with an 8.5 nm Gaussian shape corresponding to 200 fs Gaussian pulses. Though a more accurate description should include the full integral form of the nonlinear Schrödinger equation,¹² our excellent qualitative match and reasonable quantitative match validate this approach.

We measure 57% power conversion from the input pulse spectrum to the redshifted soliton for the case of 1.39 nJ input pulses to achieve ~ 0.8 nJ output soliton pulses [Fig. 2(a)]. The corresponding second-order interferometric autocorrelation (Fig. 3) gives an output pulse width of 49 fs, assuming a sech^2 pulse shape, showing a factor of four in pulse width reduction due to higher-order soliton compression (soliton order $N=2.1$) in the HOM fiber. The measured spec-

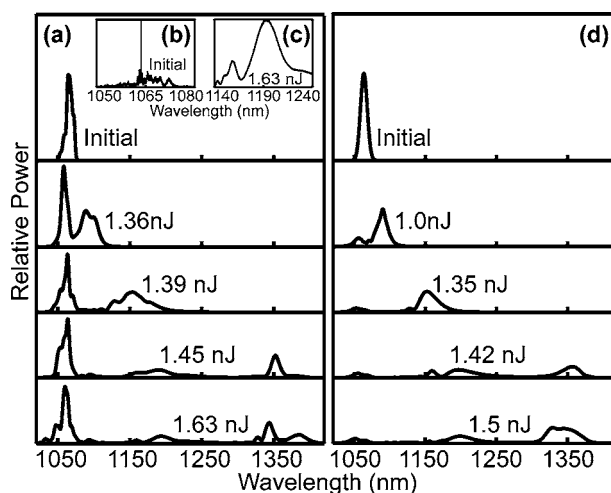


Fig. 2. (a) Soliton self-frequency shifted spectra corresponding to different input pulse energies into the HOM fiber. All traces taken at 4.0 nm resolution bandwidth (RBW). Input pulse energy noted on each trace. (b) High-resolution trace of the initial spectrum, 0.1 nm RBW. (c) High-resolution trace of the shifted soliton for 1.63 nJ input into the HOM, 0.1 nm RBW. (d) Soliton self-frequency shifted spectra calculated from simulation by using a 200 fs input Gaussian pulse and shifted soliton energies comparable with those in (a). Input pulse energy noted on each trace.

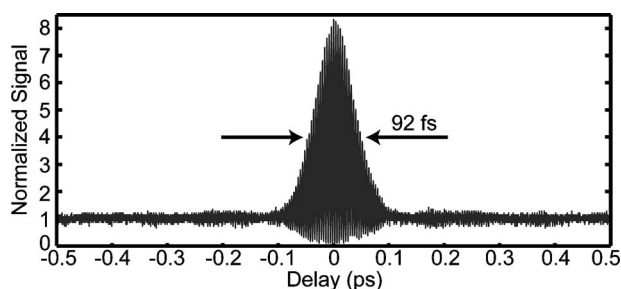


Fig. 3. Second-order interferometric autocorrelation trace of HOM output for 1.39 nJ input pulses. Autocorrelation FWHM measured to be 92 fs, corresponding to a deconvolved pulse width of 49 fs.

tral bandwidth of 35 nm gives a time–bandwidth product of 0.386, which is 23% beyond that expected for a sech^2 pulse shape. We believe the discrepancy is likely due to dispersion from ~ 5 cm of glass (collimating and focusing lenses) between the fiber output and the two-photon detector inside the autocorrelator. This explanation is supported by our numerical simulation, which gives an output pulse width of 40 fs. We further note the ripple-free, high-resolution spectrum of the shifted soliton for 1.63 nJ input [Fig. 2(c)]. This is indicative of propagation exclusively in the LP_{02} mode, since multimode propagation would surface as spectral interference.

Finally, we note the appearance of Čerenkov radiation centered about 1350 nm for 1.45 and 1.63 nJ input pulse energies [Fig. 2(a)]. Here, as has been demonstrated previously in PCFs,¹³ Čerenkov radiation is generated from phase matching between the soliton and resonant dispersive waves. This process occurs most efficiently when the soliton approaches the zero-dispersion wavelength where the dispersion slope is negative. Pumping more energy into the fiber does not redshift the soliton any further, but instead transfers the energy into the Čerenkov spectrum. As the input pulse energy is increased from 1.45 to 1.63 nJ [Fig. 2(a)], the soliton is still locked at a center wavelength of ~ 1200 nm, but more energy appears in the Čerenkov spectrum. Our simulations suggest that an ultrashort pulse can be filtered and compressed from this radiation to achieve energetic pulses across the zero-dispersion wavelength.

Though not demonstrated in our experiments, light can be easily coupled back into the fundamental mode by using another LPG at the output end. Previous work showed that by using a dispersion-matching design, ultralarge bandwidths can be supported by a LPG.¹¹ Recently conversion efficiency of 90% over a bandwidth of 200 nm was obtained for a similar fiber structure.¹⁴ Such a LPG will ensure the output pulse is always converted back to a Gaussian profile, within the tuning range. An important consideration for the output LPG is its length. Since the energetic output pulses are solitons for a specific combination of dispersion and A_{eff} of the LP_{02} mode, nonlinear distortions may occur when the energetic pulse goes to the (smaller A_{eff}) fundamental LP_{01} mode at the output. However, the length over which the signal travels in the LP_{01} mode, and hence the distortion it accumulates, can be minimized because the high-index core of the HOM fibers enable LPG lengths of < 5 mm. Note that the requirement for short LPGs actually complements the need for broad-bandwidth operation, since the conversion bandwidth is typically inversely proportional to the grating length.¹¹

Both the wavelength shift and pulse energy can be significantly increased beyond what we have demonstrated through engineering of the fiber module. For example, simple dimensional scaling of the index profile can be used to shift the dispersion curve of the LP_{02} mode. Our numerical modeling shows that an output soliton energy of approximately 2 nJ can be

realized if the dispersion curve is shifted ~ 100 nm to the longer wavelength side. Additionally, pulse energy can be scaled by increasing DA_{eff} . Aside from increasing the magnitude of dispersion through manipulation of the index profile and dimensions of the fiber, the effective area can be significantly enhanced by coupling into even higher-order modes. An effective area of $\sim 2000 \mu\text{m}^2$ (more than 40 times this HOM fiber) was recently achieved by coupling to the LP_{07} mode.¹⁴

In summary, we demonstrate SSFS between 1064 and 1200 nm in a higher-order mode, solid silica-based fiber. We are able to obtain 49 fs Raman-shifted solitons at 0.8 nJ with up to 57% power conversion efficiency. Due to the dispersion characteristics of the HOM fiber, we also observe Čerenkov radiation for appropriately energetic input pulses. We believe that HOM fiber should provide an ideal platform for achieving soliton energies from 1 to 10 nJ for SSFS at wavelengths below 1300 nm, filling the pulse energy gap between index-guided PCFs and air-core PBGFs. This intermediate pulse energy regime, which could not be reached previously for SSFS, could prove instrumental in the realization of tunable, compact, all-fiber, femtosecond sources for a wide range of practical applications.

C. Xu's e-mail address is cx10@cornell.edu.

References

1. E. M. Dianov, A. Y. Karasik, P. V. Mamyshev, A. M. Prokhorov, V. N. Serkin, M. F. Stelmakh, and A. A. Fomichev, *JETP Lett.* **41**, 294 (1985).
2. N. Nishizawa and T. Goto, *IEEE Photon. Technol. Lett.* **11**, 325 (1999).
3. M. E. Fermann, A. Galvanauskas, M. L. Stock, K. K. Wong, D. Harter, and L. Goldberg, *Opt. Lett.* **24**, 1428 (1999).
4. X. Liu, C. Xu, W. H. Knox, J. K. Chandalia, B. J. Eggleton, S. G. Kosinski, and R. S. Windeler, *Opt. Lett.* **26**, 358 (2001).
5. B. R. Washburn, S. E. Ralph, P. A. Lacourt, J. M. Dudley, W. T. Rhodes, R. S. Windeler, and S. Coen, *Electron. Lett.* **37**, 1510 (2001).
6. H. Lim, J. Buckley, A. Chong, and F. W. Wise, *Electron. Lett.* **40**, 1523 (2004).
7. F. Luan, J. C. Knight, P. S. Russell, S. Campbell, D. Xiao, D. T. Reid, B. J. Mangan, D. P. Williams, and P. J. Roberts, *Opt. Express* **12**, 835 (2004).
8. J. C. Knight, J. Arriaga, T. A. Birks, A. Ortigosa-Blanch, W. J. Wadsworth, and P. S. Russell, *IEEE Photon. Technol. Lett.* **12**, 807 (2000).
9. A. Diaspro, *Confocal and Two-Photon Microscopy* (Wiley-Liss, 2002).
10. S. Ramachandran, S. Ghalmi, J. W. Nicholson, M. F. Yan, E. Monberg, and F. V. Dimarcello, *Opt. Lett.* **31**, 2532 (2006).
11. S. Ramachandran, *J. Lightwave Technol.* **23**, 3426 (2005).
12. G. P. Agrawal, *Nonlinear Fiber Optics*, 3rd ed. (Academic, 2001).
13. D. V. Skryabin, F. Luan, J. C. Knight, and P. S. Russell, *Science* **301**, 1705 (2003).
14. S. Ramachandran, J. W. Nicholson, S. Ghalmi, M. F. Yan, P. Wisk, E. Monberg, and F. V. Dimarcello, *Opt. Lett.* **31**, 1797 (2006).